

New easy-plane $\mathbb{C}\mathbb{P}^{N-1}$ fixed points

Jonathan D’Emidio and Ribhu K. Kaul

Department of Physics & Astronomy, University of Kentucky, Lexington, KY-40506-0055

We study fixed points of the easy-plane $\mathbb{C}\mathbb{P}^{N-1}$ field theory by combining quantum Monte Carlo simulations of lattice models of easy-plane $SU(N)$ superfluids with field theoretic renormalization group calculations, by using ideas of deconfined criticality. From our simulations, we present evidence that at small N our lattice model has a first order phase transition which progressively weakens as N increases, eventually becoming continuous for large values of N . Renormalization group calculations in $4 - \epsilon$ dimensions provide an explanation of these results as arising due to the existence of an N_{ep} that separates the fate of the flows with easy-plane anisotropy. When $N < N_{ep}$ the renormalization group flows to a discontinuity fixed point and hence a first order transition arises. On the other hand, for $N > N_{ep}$ the flows are to a new easy-plane $\mathbb{C}\mathbb{P}^{N-1}$ fixed point that describes the quantum criticality in the lattice model at large N . Our lattice model at its critical point, thus gives efficient numerical access to a new strongly coupled gauge-matter field theory.

Introduction: The study of anti-ferromagnets has uncovered fascinating connections between quantum spin models and gauge theories. The connections have allowed novel gauge theoretic concepts such as deconfinement to be brought into the realm of condensed matter physics. Turning this mapping around, can the study of magnetism provide non-perturbative insights into gauge theories? Remarkably, advances in simulation algorithms for quantum anti-ferromagnets [1] have recently allowed controlled numerical access to otherwise poorly understood strongly coupled gauge theories; the most prominent example being the $\mathbb{C}\mathbb{P}^{N-1}$ gauge theory proposed for deconfined critical points (DCP) in $SU(N)$ magnets [2].

In early work on DCP, a prominent role was played by the “easy-plane $SU(2)$ ” [3] magnet and its corresponding “easy-plane $\mathbb{C}\mathbb{P}^1$ ” field theory [2, 4]. A self-duality in the field theory suggested that this could be the best candidate for a deconfined critical point [5]. Subsequent numerical work has concluded however that this transition is first order, both in direct discretizations of the field theory [6, 7] as well as in simulations of the quantum anti-ferromagnet [8]. The easy-plane case is in contrast to the symmetric $SU(N)$ case (we refer to this as s- $SU(N)$), where striking agreement between technical field theoretic calculations [9–12] and numerical simulations of the quantum magnets has been demonstrated [13–15].

The sharp contrast between the easy-plane and symmetric cases has been unexplained so far. In this work we address the first order transition in the easy-plane case using both lattice simulations of an ep- $SU(N)$ model as well as renormalization group calculations on a proposed ep- $\mathbb{C}\mathbb{P}^{N-1}$ field theory. We find the first order transition in the ep- $SU(N)$ models found for $N = 2$ in previous work persists for larger N . A careful analysis however shows that the first order jump quantitatively weakens as N increases. Renormalization group ϵ -expansion calculations find that the field theory hosts a new ep- $\mathbb{C}\mathbb{P}^{N-1}$ fixed point only for $N > N_{ep}$, suggesting that the transition can eventually become continuous. Consistent with this result, we find that the transition in our lattice model

turns continuous around $N \approx 20$. For $N = 21$ we provide a detailed scaling analysis of our numerical data that confirms a continuous transition in a new universality class. Our work clarifies and significantly extends the discussion of the DCP phenomena in easy-plane magnets and its relation to the symmetric case.

Easy-plane model & field theory: We consider a family of bipartite ep- $SU(N)$ spin models introduced recently by us [8], they are extensions of the quantum XY model to larger N . They are written in terms of the T_i^a , the fundamental generators of $SU(N)$ on site i :

$$H = -\frac{J_{1\perp}}{N} \sum_{a, \langle ij \rangle} ' T_i^a T_j^{a*} - \frac{J_{2\perp}}{N} \sum_{a, \langle\langle ij \rangle\rangle} ' T_i^a T_j^a. \quad (1)$$

the \sum' denotes the sum on a is restricted to the $N^2 - N$ off-diagonal generators (a sum on all generators a would give the s- $SU(N)$ model). The $\langle ij \rangle$ ($\langle\langle ij \rangle\rangle$) indicates nearest (next nearest) neighbors on the square lattice which are on opposite (same) sublattices and in conjugate (same) representations. The model H is an easy plane deformation of the s- $SU(N)$ J_1 - J_2 model [13], it has a global $U(1)^{N-1} \times S_N$ in addition to time reversal and lattice symmetries. The model harbors in its phase diagram the SF-VBS transition for all $N > 5$. H is Marshall positive; we hence simulate it with stochastic series Monte Carlo on $L \times L$ lattice at an inverse temperature β [16].

The effective field theory for SF-VBS phase transition in the ep- $SU(N)$ model is obtained by applying the ideas of DCP [2, 4] to Eq. (1). The theory “ep- $\mathbb{C}\mathbb{P}^{N-1}$ ” is a sum of kinetic and potential terms $\mathcal{L}_{ep} = \mathcal{L}_1 + \mathcal{L}_2$,

$$\begin{aligned} \mathcal{L}_1 &= \sum_{\alpha} |(\partial_{\mu} - ieA_{\mu})z_{\alpha}|^2 + \frac{1}{2}(\vec{\nabla} \times \vec{A})^2 \\ \mathcal{L}_2 &= r \sum_{\alpha} |z_{\alpha}|^2 + \frac{u}{2} \left(\sum_{\alpha} |z_{\alpha}|^2 \right)^2 + \frac{v}{2} \sum_{\alpha} |z_{\alpha}|^4, \end{aligned} \quad (2)$$

where the z_{α} are N complex fields coupled to a $U(1)$ gauge field, A_{μ} . The term v breaks the full s- $SU(N)$ sym-

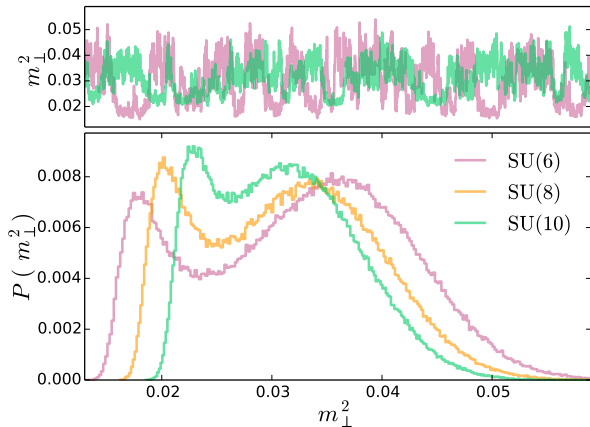


FIG. 1. First order transitions for moderate values of N . The upper panels shows MC histories (arbitrary units) of the estimator for m_{\perp}^2 for $N = 6$ and 10 . The bottom panel shows histograms of m_{\perp}^2 taken at $L = 50$ for $J_2/J_1 \equiv g = 0.250, 0.876, 1.58$ for $N = 6, 8, 10$ respectively, clearly showing double peaked behavior. This data was collected with $\beta = 1.5L$.

metry of the $s\text{-}\mathbb{C}\mathbb{P}^{N-1}$ model to a $U(1)^{N-1} \times S_N$ (what we shall call ep-SU(N)). It is known from the large- N expansion [17] that for N larger than some finite N_s , in $d = 3$ the $s\text{-}\mathbb{C}\mathbb{P}^{N-1}$ field theory has a finite coupling fixed point (FP). Based on various numerical studies it is now believed that most likely $N_s < 2$, so that Eq. 2 has a FP for all values of N (see [18] for a nice summary). A central issue we address here is the fate of these FPs when easy-plane anisotropy v is introduced.

Weakening first-order transition: We begin with a numerical study of Eq. (1). We have shown in [8] that the ep-SU(N) models map to a certain loop model. We can hence calculate two useful quantities to probe magnetic ordering: the average of the square of the spatial winding number of the loops $\langle W^2 \rangle$ and a normalized magnetic order parameter $m_{\perp}^2 = \frac{1}{(1-1/N)N_{\text{site}}^2} \sum_a \sum_{i,j} \langle \tilde{T}_i^a \tilde{T}_j^a \rangle$ (where the sum on a is on the off-diagonal generators, i and j are summed on the entire lattice and $\tilde{T} = T(T^*)$ on the A(B) sublattice), which although off-diagonal in the $|\alpha\rangle$ basis can be estimated by measuring a particular statistical property of the loops [19]. We have normalized m_{\perp}^2 so that the maximum value it can take is 1 for all N , allowing for a meaningful comparison across different N .

Previously we found that the SF-VBS transition is first order for $N \leq 5$ [8]. In Fig. 1 we present data that shows the first order behavior persists as N is increased up to $N = 10$. A hitherto unanswered but important question is whether the first order jump weakens as N increases. We find evidence in favor of this assertion, since the histogram peaks get closer as N is increased. Beyond $N \approx 16$ we have found no evidence for double peaked histograms. To carry out a more quantitative analysis,

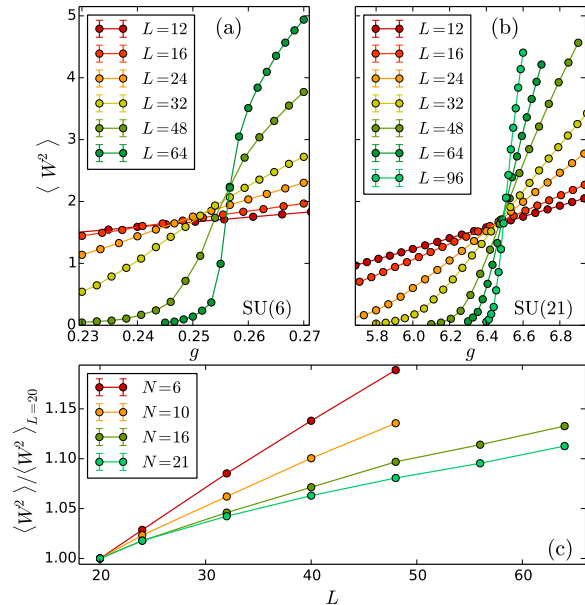


FIG. 2. Scaling of the spatial winding number square $\langle W^2 \rangle$. (a) Crossing for $N = 6$. (b) Crossing for $N = 21$. (c) Value at the L and $L/2$ crossing of $\langle W^2 \rangle$ for a range of N normalized to the crossing value at $L = 20$ for each N . For the smaller N a clear linear divergence is seen as expected for a first-order transition (ergodicity issues limit the system sizes here). For larger N a slow growth is observed very similar to what has been studied in detail for the $s\text{-SU}(2)$ case and interpreted as evidence for a continuous transition with two length scales [21], like we have here. All the data was taken at $\beta = 6L$ which is in the $T = 0$ regime [19].

which has been popular in the study of the DCPs [6], we turn to $\langle W^2 \rangle$ (which is related to the spin stiffness as $\beta\rho_s$). At a first order transition one expects a linear divergence of $\langle W^2 \rangle$ as one approaches the phase transition since ρ_s stays finite. Any sub-linear behavior indicates that the transition is continuous since ρ_s vanishes in the thermodynamic limit [20]. In Fig. 2 we present a study of the crossing of $\langle W^2 \rangle$. We find clear evidence for the expected linear behavior at moderate values of N . As N is increased beyond about $N \approx 16$ we find a very slow growth of $\langle W^2 \rangle$ inconsistent with linear behavior but consistent with what has been found in $s\text{-SU}(N)$ models, where the transition is believed to be continuous [20, 21]. This study provides clear evidence that the first-order jump decreases as N increases, possibly becoming continuous.

Renormalization group analysis: The weakening of the first-order SF-VBS transitions at larger N raises important questions: Is the transition first order for all N or does it become continuous beyond some finite N_{ep} ? If the transition becomes continuous: Is it truly a new uni-

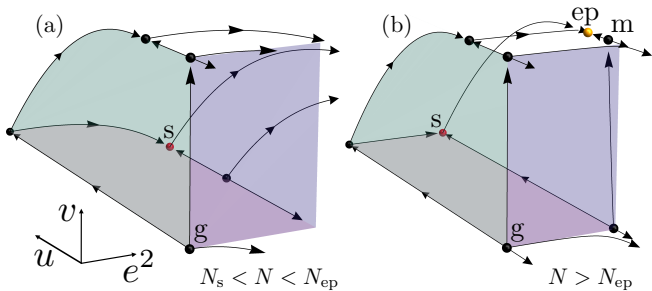


FIG. 3. Renormalization group flows of the ep- \mathbb{CP}^{N-1} model for (a) $N_s < N < N_{ep}$ and (b) $N > N_{ep}$ at leading order in $4 - \epsilon$ dimensions obtained by numerical integration of Eq.(3). Fixed points are shown as bold dots, we have only labeled a few significant to our discussion. The flows in the $v = 0$ plane have been obtained previously [17] and include the “s” fixed point that describes DCP in s-SU(N) models [19]. While the flows have many FPs [19], a DCP of the ep-SU(N) spin model must have all three eigen-directions in the e^2 - u - v irrelevant. For $N < N_{ep}$ there are no such FPs; there is hence a runaway flow to a first order transition. For $N > N_{ep}$ two FPs emerge: “m” is multicritical and “ep” is the new ep-DCP that describes the SF-VBS transition (yellow dot). The gaussian fixed point at the origin has been labeled “g” for clarity. More details are in the SM [19].

versality class of an ep- \mathbb{CP}^{N-1} or does the anisotropy become irrelevant at the s-FP resulting in s- \mathbb{CP}^{N-1} criticality for the “easy-plane” models?

To answer these questions, we compute the RG flows of Eq. (2) in $4 - \epsilon$ dimensions. We will work in the critical plane where $r = 0$, the r operator being strongly relevant at tree level will continue to be relevant in the ϵ -expansion. To leading order (assuming u, v and e^2 are $\mathcal{O}(\epsilon)$), we find the following RG equations,

$$\begin{aligned} \frac{de^2}{d\ln s} &= \epsilon e^2 - \frac{N}{3} e^4, \\ \frac{du}{d\ln s} &= \epsilon u - (N+4)u^2 - 4uv - 6e^4 + 6e^2u, \\ \frac{dv}{d\ln s} &= \epsilon v - 5v^2 - 6uv + 6e^2v, \end{aligned} \quad (3)$$

which for $v = 0$ reduce to the well known RG equations for the s- \mathbb{CP}^{N-1} model [17, 22]. Given the relevance of r , a generic critical point of ep- \mathbb{CP}^{N-1} would be a fixed point of Eq. (3) with all three eigen-directions in e^2 - u - v -space irrelevant. The FP structure and flows of Eq. (3) (shown in Fig. 3) change at two values of N : N_s and N_{ep} with $N_s < N_{ep}$. For $N < N_s$ [not shown] there are no FPs with $e^2 \neq 0$ and a generic flow runs away to a first order transition. For $N > N_s$ a $v = 0$ FP “s” appears, which describes the s-SU(N) DCP phenomena, but at which v is always relevant. There are two distinct fates of the flow with $v \neq 0$: For $N_s < N < N_{ep}$ [see Fig. 3(a)] v causes a runaway flow to a discontinuity FP, i.e. the phase transition turns first order. On the other hand, for $N > N_{ep}$ [see Fig. 3(b)] a new fixed point “ep” appears.

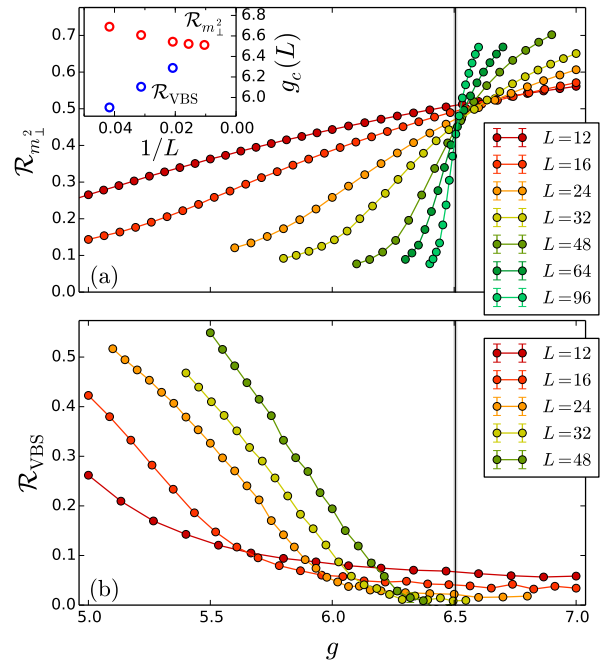


FIG. 4. Correlation ratios close to the phase transition for $N = 21$. (a) The SF order parameter ratio, $R_{m,1/2}$ shows good evidence for a continuous transition with a nicely convergent crossing point of $g = 6.505(5)$. (b) R_{VBS} shows a crossing point that converges to the same value of the critical coupling. We note however that the crossing converges much more slowly (see text). The inset shows the convergence of the crossings points of L and $L/2$ of SF and VBS ratios. Note their convergence to a common critical coupling indicating a direct transition.

At this FP all eigen-directions in the $e^2 - u - v$ space are irrelevant and hence r is the only relevant perturbation. “ep” hence describes a generic continuous deconfined SF-VBS transition in models of the form Eq. (1). In the leading order of the ϵ -expansion we have $N_s \approx 183$ [17] and $N_{ep} \approx 5363$ (independent of ϵ). From previous work on the symmetric case, it is well known that these leading order estimates are unreliable in $d = 3$: Indeed, in the next to leading order, N_s becomes negative for $\epsilon = 1$ [23, 24]. Ultimately the values of $N_{s,ep}$ must be obtained from numerical simulations. Nonetheless, it is expected that the basic structure of fixed points and flows obtained here using the ϵ -expansion are reliable. Based on our study, we make the following conclusions: Even in a regime where there is a symmetric fixed point ($N > N_s$), for $N_s < N < N_{ep}$, easy-plane anisotropy will drive the DCP first-order. For $N > N_{ep}$ a new FP emerges. Easy-plane anisotropy then results in a continuous SF-VBS transition in a new ep- \mathbb{CP}^{N-1} universality class.

Study of fixed point: Having presented evidence from the ϵ -expansion that with increasing N the transition

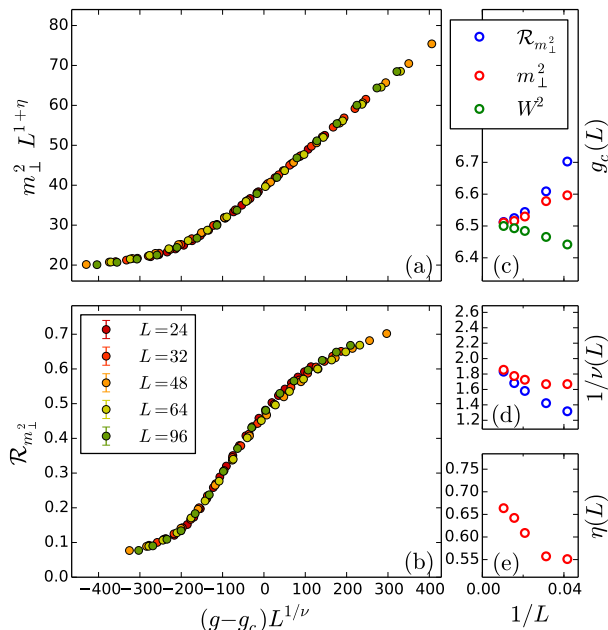


FIG. 5. Data collapse for the SF order parameter at $N = 21$. (a) Finite size data collapsed to $m_{\perp}^2 = L^{-(1+\eta_{\text{SF}})} \mathbb{M}[(g - g_c)L^{1/\nu}]$ with parameters $g_c=6.511$, $\nu=0.556$ ($1/\nu = 1.795$), $\eta=0.652$. (b) Collapse of ratio $R_{m_{\perp}^2} = \mathbb{R}[(g - g_c)L^{1/\nu}]$ with parameters $g_c=6.518$, $\nu=0.582$ ($1/\nu = 1.719$). The side panels shows convergence of estimates for various quantities from the collapse of L and $L/2$ data: (c) the critical coupling $g_c = 6.505(1)$ from pair-wise collapses of m_{\perp}^2 and $R_{m_{\perp}^2}$, as well as crossings of $\langle W^2 \rangle$ (see Fig. 2) for data. Panel (d) shows $1/\nu(L)$, which we estimate to converge to $1/\nu = 2.3(2)$. Likewise we estimate $\eta(L)$ to converge to $\eta = 0.72(3)$, which is shown in panel (e).

should turn continuous and in a new universality class, it is of interest to study the scaling behavior at large N . We will focus on $N = 21$ where we have found no evidence for first order behavior on the largest system sizes that we have access to. We construct dimensionless ratios $\mathcal{R}_{m_{\perp}^2}$ and \mathcal{R}_{VBS} which go to 1(0) in their respective ordered (disordered) phases. Fig. 4 shows our data for $N = 21$. The large correction to scaling observed in the VBS data are expected: according to the DCP theory the VBS anomalous dimension $\eta_{\text{VBS}} \propto N$ which causes the leading VBS correlation functions to decay very rapidly at this large value of N . This makes it hard to separate the leading and sub-leading behavior on the available system sizes. Since the SF data shows a good crossing, we carry out a full scaling analysis in Fig. 5. The data for both m_{\perp}^2 and $R_{m_{\perp}^2}$ collapse nicely without the inclusion of corrections to scaling. They lead to consistent values of critical couplings and scaling dimensions lending sup-

port for a continuous transition ep- \mathbb{CP}^{N-1} fixed point emerging at large N .

In conclusion, we have studied new lattice models for deconfined criticality with easy-plane $\text{SU}(N)$ symmetry. We find persistent first order behavior in these lattice models at small to intermediate N , in sharp contrast to the continuous transitions found in the symmetric models for the same range of N . As N increases the first order easy-plane transition weakens and eventually becomes continuous. Our RG flows provide a way to understand both the first-order and shift to continuous transitions: The easy-plane anisotropy is always relevant at the symmetric \mathbb{CP}^{N-1} fixed point, for $N < N_{ep}$ there is no easy-plane fixed point and hence the anisotropy drives the transition first order. For $N > N_{ep}$ a new fixed point emerges resulting in a continuous transition in a new “easy-plane”- \mathbb{CP}^{N-1} universality class which is an example of a strongly coupled gauge-matter field theory. Our lattice model provides a sign-free discretization of this field theory that is amenable to efficient numerical simulations. We leave for future work the determination of a precise value of N_{ep} , comparisons of the universal quantities with easy-plane large- N expansions, and a comparative study of the scaling corrections between the easy-plane and symmetric cases. It would be of interest to complement our work with studies of field theories such as Eq. (2) using the conformal bootstrap [25].

Acknowledgements: We thank G. Murthy for many discussions. Partial financial support was received through NSF DMR-1611161 and the MacAdam fellowship. The numerical simulations reported in the manuscript were carried out on the DLX cluster at the University of Kentucky.

-
- [1] R. K. Kaul, R. G. Melko, and A. W. Sandvik, *Annu. Rev. Cond. Matt. Phys.* **4**, 179 (2013), URL <http://www.annualreviews.org/doi/abs/10.1146/annurev-conmatphys-030212-184215>.
 - [2] T. Senthil, A. Vishwanath, L. Balents, S. Sachdev, and M. P. A. Fisher, *Science* **303**, 1490 (2004), URL <http://www.sciencemag.org/content/303/5663/1490.abstract>.
 - [3] A. W. Sandvik, S. Daul, R. R. P. Singh, and D. J. Scalapino, *Phys. Rev. Lett.* **89**, 247201 (2002), URL <http://link.aps.org/doi/10.1103/PhysRevLett.89.247201>.
 - [4] T. Senthil, L. Balents, S. Sachdev, A. Vishwanath, and M. P. A. Fisher, *Phys. Rev. B* **70**, 144407 (2004), URL <http://link.aps.org/doi/10.1103/PhysRevB.70.144407>.
 - [5] O. I. Motrunich and A. Vishwanath, *Phys. Rev. B* **70**, 075104 (2004), URL <http://link.aps.org/doi/10.1103/PhysRevB.70.075104>.
 - [6] A. Kuklov, N. Prokofev, B. Svistunov, and M. Troyer, *Annals of Physics* **321**, 1602 (2006), ISSN 0003-4916, July 2006 Special Issue, URL

- <http://www.sciencedirect.com/science/article/pii/S0003491606000789>.
- [7] S. Kragset, E. Smørgrav, J. Hove, F. S. Nogueira, and A. Sudbø, Phys. Rev. Lett. **97**, 247201 (2006), URL <http://link.aps.org/doi/10.1103/PhysRevLett.97.247201>.
- [8] J. D'Emidio and R. K. Kaul, Phys. Rev. B **93**, 054406 (2016), URL <http://link.aps.org/doi/10.1103/PhysRevB.93.054406>.
- [9] G. Murthy and S. Sachdev, Nucl. Phys. B **344**, 557 (1990).
- [10] E. Dyer, M. Mezei, S. S. Pufu, and S. Sachdev, Journal of High Energy Physics **2015**, 1 (2015), ISSN 1029-8479, URL [http://dx.doi.org/10.1007/JHEP06\(2015\)037](http://dx.doi.org/10.1007/JHEP06(2015)037).
- [11] R. K. Kaul and S. Sachdev, Phys. Rev. B **77**, 155105 (2008), URL <http://link.aps.org/doi/10.1103/PhysRevB.77.155105>.
- [12] T. Senthil and M. P. A. Fisher, Phys. Rev. B **74**, 064405 (2006), URL <http://link.aps.org/doi/10.1103/PhysRevB.74.064405>.
- [13] R. K. Kaul and A. W. Sandvik, Phys. Rev. Lett. **108**, 137201 (2012), URL <http://link.aps.org/doi/10.1103/PhysRevLett.108.137201>.
- [14] M. S. Block, R. G. Melko, and R. K. Kaul, Phys. Rev. Lett. **111**, 137202 (2013), URL <http://link.aps.org/doi/10.1103/PhysRevLett.111.137202>.
- [15] A. Nahum, P. Serna, J. T. Chalker, M. Ortuño, and A. M. Somoza, Phys. Rev. Lett. **115**, 267203 (2015), URL <http://link.aps.org/doi/10.1103/PhysRevLett.115.267203>.
- [16] A. W. Sandvik, AIP Conf. Proc. **1297**, 135 (2010), URL <http://scitation.aip.org/content/aip/proceeding/aipcp/10.1063/1.3518900>.
- [17] B. I. Halperin, T. C. Lubensky, and S.-k. Ma, Phys. Rev. Lett. **32**, 292 (1974), URL <http://link.aps.org/doi/10.1103/PhysRevLett.32.292>.
- [18] A. Nahum, J. T. Chalker, P. Serna, M. Ortuño, and A. M. Somoza, Phys. Rev. X **5**, 041048 (2015), URL <http://link.aps.org/doi/10.1103/PhysRevX.5.041048>.
- [19] Please refer to Supplemental Materials for further details of the numerical simulations.
- [20] R. K. Kaul, Phys. Rev. B **84**, 054407 (2011), URL <http://journals.aps.org/prb/abstract/10.1103/PhysRevB.84.054407>.
- [21] H. Shao, W. Guo, and A. W. Sandvik, **352**, 213 (2016), ISSN 0036-8075, URL <http://science.sciencemag.org/content/352/6282/213>.
- [22] I. Herbut, *A Modern Approach to Critical Phenomena* (Cambridge University Press, 2010).
- [23] S. Kolnberger and R. Folk, Phys. Rev. B **41**, 4083 (1990), URL <http://link.aps.org/doi/10.1103/PhysRevB.41.4083>.
- [24] I. F. Herbut and Z. Tes̃anović, Phys. Rev. Lett. **78**, 980 (1997), URL <http://link.aps.org/doi/10.1103/PhysRevLett.78.980>.
- [25] S. El-Showk, M. F. Paulos, D. Poland, S. Rychkov, D. Simmons-Duffin, and A. Vichi, Phys. Rev. D **86**, 025022 (2012), URL <http://link.aps.org/doi/10.1103/PhysRevD.86.025022>.
- [26] O. F. Syljuåsen and A. W. Sandvik, Phys. Rev. E **66**, 046701 (2002).
- [27] A. Dorneich and M. Troyer, Phys. Rev. E **64**, 066701 (2001), URL <http://link.aps.org/doi/10.1103/PhysRevE.64.066701>.
- [28] M. Peskin and D. Schroeder, *An Introduction to Quantum Field Theory*, Advanced book classics (Addison-Wesley Publishing Company, 1995), ISBN 9780201503975, URL <https://books.google.com/books?id=i35LALNOGosC>.
- [29] P. M. Chaikin and T. C. Lubensky, *Principles of Condensed Matter Physics* (Cambridge University Press, 2000).

SUPPLEMENTAL MATERIALS

Lattice Hamiltonian

We elaborate on the spin Hamiltonian (1), which can be simply written in terms of its matrix elements (choosing the normalization $\text{Tr}[T^a T^b] = \delta_{ab}$)

$$H = -\frac{J_{1\perp}}{N} \sum_{\langle ij \rangle, \alpha, \beta, \alpha \neq \beta} |\alpha_i \alpha_j\rangle \langle \beta_i \beta_j| - \frac{J_{2\perp}}{N} \sum_{\langle\langle ij \rangle\rangle, \alpha, \beta, \alpha \neq \beta} |\alpha_i \beta_j\rangle \langle \beta_i \alpha_j|, \quad (4)$$

where here we emphasize that α and β are summed from 1 to N with the constraint that $\alpha \neq \beta$. The symmetry of this model is global phase rotations of the form $|\alpha\rangle \rightarrow e^{i\theta_\alpha} |\alpha\rangle$, where on one sublattice the phase is conjugated due to the representation. This gives $U(1)^{N-1}$ since an overall phase is trivial. There is also a discrete permutation symmetry S_N that corresponds to a relabeling of the colors. We note that dropping the constraint $\alpha \neq \beta$ restores the full $SU(N)$ symmetry and corresponds to a model already studied in the context of deconfined criticality at large N [13].

This model is explicitly sign free and is amenable to quantum Monte Carlo techniques. We have used the stochastic series expansion QMC algorithm [26], which samples the partition function at finite temperature. For practical implementation, one needs to add a constant to the Hamiltonian in order to generate diagonal matrix elements. We find it convenient to add diagonals with the same weight as the off-diagonals, as follows:

$$H \rightarrow -\frac{J_{1\perp}}{N} \sum_{\langle ij \rangle} \left(\sum_{\alpha, \beta, \alpha \neq \beta} |\alpha_i \alpha_j\rangle \langle \beta_i \beta_j| + \mathbb{1} \right) - \frac{J_{2\perp}}{N} \sum_{\langle\langle ij \rangle\rangle} \left(\sum_{\alpha, \beta, \alpha \neq \beta} |\alpha_i \beta_j\rangle \langle \beta_i \alpha_j| + \mathbb{1} \right). \quad (5)$$

We refer the reader to more details of the loop algorithm contained in [8]. One notable aspect of this $J_{1\perp} - J_{2\perp}$ model is that the addition of the $J_{2\perp}$ term can be treated with minimal extra effort, given a code that simulates $J_{1\perp}$ only. Updating a matrix element (vertex) associated with $J_{2\perp}$ can be achieved by first time reversing the spin states on one sublattice of the vertex, then scattering through the vertex according to the rules for $J_{1\perp}$ matrix elements, and finally reversing the spins back.

Measurements

Many of our measurements are part of the standard tool kit. This includes the winding number fluctuation $\langle W^2 \rangle$, which is related to the superfluid stiffness $\rho = \langle W^2 \rangle / \beta$; and also the equal-time bond-bond correlation function, which is used to construct \mathcal{R}_{VBS} . In order to introduce the VBS order parameter and ratio, we first consider the Fourier transformed bond-bond correlator

$$\tilde{C}_{VBS}^a(\vec{q}) = \frac{1}{N_{\text{site}}^2} \sum_{\vec{r}, \vec{r}'} e^{i(\vec{r} - \vec{r}') \cdot \vec{q}} \langle \tilde{P}_{\vec{r}a} \tilde{P}_{\vec{r}'a} \rangle, \quad (6)$$

where $\tilde{P}_{\vec{r}a}$ is an off-diagonal nearest neighbor bond operator of the form $\sum_{\alpha, \beta, \alpha \neq \beta} |\alpha\alpha\rangle_{ij} \langle \beta\beta|_{ij}$ that acts at a bond location \vec{r} with orientation $a \in \{x, y\}$.

For columnar VBS patterns, peaks appear at the momenta $(\pi, 0)$ and $(0, \pi)$ for x and y -oriented bonds, respectively. The VBS order parameter is thus given by

$$\mathcal{O}_{VBS} = \frac{\tilde{C}_{VBS}^x(\pi, 0) + \tilde{C}_{VBS}^y(0, \pi)}{2}. \quad (7)$$

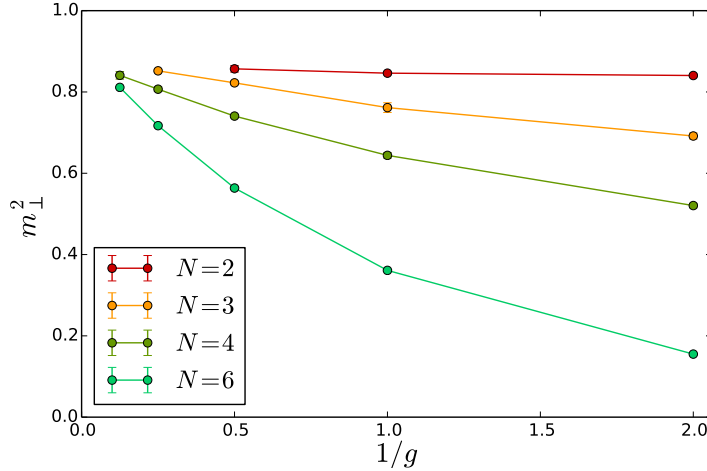


FIG. 6. Maximum values of m_{\perp}^2 deep in the superfluid phase for different values of N . Each data point was obtained by extrapolating the value of m_{\perp}^2 in the thermodynamic limit at a fixed value of the coupling $g = J_{2\perp}/J_{1\perp}$. Increasing g drives the system into the superfluid phase, we can thus observe the maximum possible value of m_{\perp}^2 in the limit $1/g \rightarrow 0$. The data is consistent with an upper bound of one.

We can further construct the VBS ratio, which is defined as

$$\mathcal{R}_{VBS}^x = 1 - \tilde{C}_{VBS}^x(\pi + 2\pi/L, 0) / \tilde{C}_{VBS}^x(\pi, 0) \quad (8)$$

And similarly for \mathcal{R}_{VBS}^y with all of the q_x and q_y arguments swapped. We then average over x and y -orientations.

$$\mathcal{R}_{VBS} = \frac{\mathcal{R}_{VBS}^x + \mathcal{R}_{VBS}^y}{2}. \quad (9)$$

This quantity goes to 1 in a phase with long-range VBS order, and approaches 0 in the superfluid phase. It is thus a useful crossing quantity that allows us to locate the transition.

To construct these quantities, we measure the equal time bond-bond correlation function in QMC with the following estimator

$$\langle \Theta_1 \Theta_2 \rangle = \frac{1}{\beta^2} \langle (n-1)! N[\Theta_1, \Theta_2] \rangle \quad (10)$$

where Θ_1 and Θ_2 are any two QMC operators (in our case off-diagonal nearest neighbor bond operators), n is the number of non-null operators in the operator string, and $N[\Theta_1, \Theta_2]$ is the number of times Θ_1 and Θ_2 appear in sequence in the operator string (excluding null slots).

In this work we have also made use of the less common “in-plane” magnetization m_{\perp}^2 , for which we have produced magnetic data collapses. We now outline this particular measurement. The reader is directed to [27] for more details.

The superfluid (magnetic) ordering in our system is off-diagonal in the computational basis, meaning that the relevant equal-time correlation functions are of the form $\langle S_i^+ S_j^- \rangle$, written in terms of raising and lowering spin operators. The placement of such an operator into a QMC configuration will in general give zero, unless the two operators are joined by a loop of a certain color. Loop updates can be regarded as inserting a raising and lowering pair (defects) at the same time slice and spatial location, then propagating one of the defects until it annihilates with the first, forming a closed loop. The algorithm is stochastically sampling the space of allowed configurations with two defects. The measurement $\langle S_i^+ S_j^- \rangle$ is then given by the average number of times these two defects occur at the same time slice at locations i and j , which is averaged over the total number of loops grown. We note that starting loops at a vertex leg will bias this measurement, so it must be performed by choosing a random time slice and spatial location in which to start the loop.

We normalize the (0,0) component of the correlation function to the value $N - 1 = \sum_a T^a T^a$, where the sum on a is on the off-diagonal generators. This is due to the fact that we have chosen $\text{Tr}[T^a T^b] = \delta_{ab}$. We then construct m_{\perp}^2 based on the off-diagonal correlation function as follows:

4×4	$N = 2$	$J_{1\perp} = 1.0$	$J_{2\perp} = 1.0$
e_{ex}	-1.082912818	$m_{\perp\text{ex}}^2$	1.110134109
e_{QMC}	-1.082909(4)	$m_{\perp\text{QMC}}^2$	1.11014(1)
4×4	$N = 2$	$J_{1\perp} = 1.0$	$J_{2\perp} = 2.0$
e_{ex}	-1.629091615	$m_{\perp\text{ex}}^2$	1.107517598
e_{QMC}	-1.629086(5)	$m_{\perp\text{QMC}}^2$	1.10753(1)
4×2	$N = 3$	$J_{1\perp} = 1.0$	$J_{2\perp} = 1.0$
e_{ex}	-1.131110222	$m_{\perp\text{ex}}^2$	1.408846135
e_{QMC}	-1.131100(5)	$m_{\perp\text{QMC}}^2$	1.408849(6)
4×2	$N = 3$	$J_{1\perp} = 1.0$	$J_{2\perp} = 2.0$
e_{ex}	-1.618465034	$m_{\perp\text{ex}}^2$	1.423156633
e_{QMC}	-1.618476(7)	$m_{\perp\text{QMC}}^2$	1.423150(8)

TABLE I. QMC versus exact diagonalization. For brevity we provide just the energy per site and normalized m_{\perp}^2 for $N = 2$ and $N = 3$ systems. We have used $\beta = 32$ in our QMC simulations.

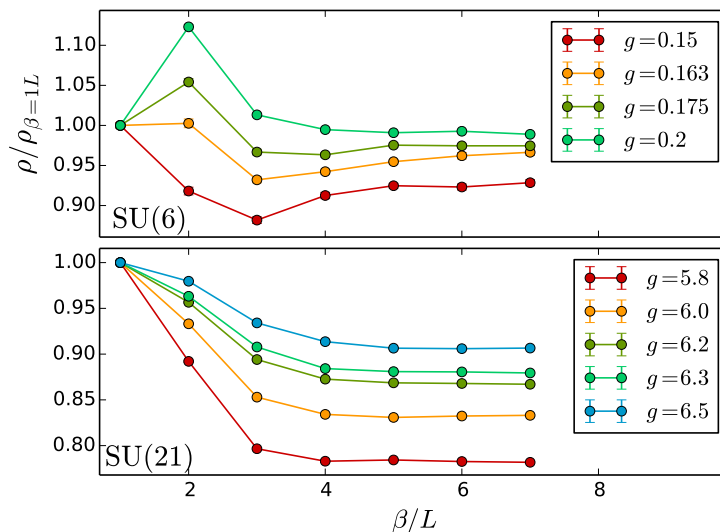


FIG. 7. Convergence of the superfluid stiffness (ρ) as a function of β for $L = 16$ around transition. Finite temperature effects are absent when $\beta \approx 5L$ for both SU(6) and SU(21). We therefore conservatively fix $\beta = 6L$ for the crossing analysis and data collapse presented in the main paper.

$$m_{\perp}^2 = \frac{1}{(1 - \frac{1}{N})N_{\text{site}}^2} \sum_a' \sum_{i,j} \langle \tilde{T}_i^a \tilde{T}_j^a \rangle \quad (11)$$

where i and j are summed on the entire lattice and $\tilde{T} = T(T^*)$ on the A(B) sublattice. In practice we use lattice symmetries to reduce the number of correlators that need to be stored. Here we have importantly chosen an overall normalization factor for m_{\perp}^2 such that the upper bound in the ordered phase is equal to one for all N . The factor $(1 - 1/N) = (N - 1)/N$ accounts for the fact that the generators have been normalized such that the (0,0) component of the correlator is $N - 1$ and that, given a color at location 0, the probability of picking the same color at long distances is $1/N$. This amounts to saying that the most magnetically ordered configurations consist of only N loops (one for each color).

The normalization allows us to meaningfully compare this measurement across different values of N and observe a reduction in the size of the first-order jump as in Fig. 1. We demonstrate that this normalization is correct in Fig. 6 by extrapolating the value of m_{\perp}^2 in the thermodynamic limit for different values of $g = J_{2\perp}/J_{1\perp}$.

Analogous to the VBS ratio, we can construct the magnetic ratio as well ($\mathcal{R}_{m_{\perp}^2}$). If we denote the Fourier transformed off-diagonal spin-spin correlator as

$$\tilde{C}_{m_{\perp}^2}(\vec{q}) = \frac{1}{(1 - \frac{1}{N})N_{\text{site}}^2} \sum_a' \sum_{\vec{r}, \vec{r}'} e^{i(\vec{r} - \vec{r}') \cdot \vec{q}} \langle \tilde{T}_{\vec{r}}^a \tilde{T}_{\vec{r}'}^a \rangle, \quad (12)$$

then the magnetic ratio is then given by

$$\mathcal{R}_{m_{\perp}^2} = 1 - \frac{\tilde{C}_{m_{\perp}^2}(2\pi/L, 0) + \tilde{C}_{m_{\perp}^2}(0, 2\pi/L)}{2\tilde{C}_{m_{\perp}^2}(0, 0)}. \quad (13)$$

We have thoroughly checked all of our measurements against exact diagonalization on small system sizes. In Table I we provide comparisons of the energy per site and normalized m_{\perp}^2 between QMC and exact diagonalization, showing agreement within the statistical error.

In order to avoid finite temperature effects in our crossing analysis and data collapse, we fixed $\beta = 6L$ in those simulations. This value was chosen based on the zero temperature convergence of the superfluid stiffness $\rho = \langle W^2 \rangle / \beta$ on an $L = 16$ system size for $N = 6$ and $N = 21$ around the transition. This data is shown in Fig. 7.

Renormalization group methods

We refer the reader to [22], which is a useful reference that outlines in detail many of the results that we will now discuss. We have performed momentum shell renormalization group transformations in $4 - \epsilon$ dimensions with the Lagrangian density (2). We therefore as a starting point write the Euclidean action in k -space as follows:

$$\begin{aligned} S = & \sum_{\alpha} \int \frac{d\vec{k}}{(2\pi)^d} (\vec{k}^2 + r) z_{\alpha}^*(\vec{k}) z_{\alpha}(\vec{k}) \\ & - e \sum_{\alpha} \int \frac{d\vec{k} d\vec{p}}{(2\pi)^{2d}} (2\vec{k} + \vec{p}) \cdot \vec{A}(\vec{p}) z_{\alpha}^*(\vec{p} + \vec{k}) z_{\alpha}(\vec{k}) \\ & + e^2 \sum_{\alpha} \int \frac{d\vec{k} d\vec{p} d\vec{q}}{(2\pi)^{3d}} \vec{A}(\vec{p}) \cdot \vec{A}(\vec{q}) z_{\alpha}^*(\vec{p} + \vec{q} + \vec{k}) z_{\alpha}(\vec{k}) \\ & + \frac{1}{2} \sum_{\alpha, \beta} (u + v\delta_{\alpha\beta}) \int \frac{d\vec{k}_1 \dots d\vec{k}_4}{(2\pi)^{3d}} \delta^d(\vec{k}_1 - \vec{k}_2 + \vec{k}_3 - \vec{k}_4) z_{\alpha}^*(\vec{k}_1) z_{\alpha}(\vec{k}_2) z_{\beta}^*(\vec{k}_3) z_{\beta}(\vec{k}_4) \\ & + \frac{1}{2} \sum_{i,j} \int \frac{d\vec{k}}{(2\pi)^d} A_i(\vec{k}) [\vec{k}^2 (\delta_{ij} - \hat{k}_i \hat{k}_j) + \frac{k_i k_j}{\xi}] A_j(-\vec{k}). \end{aligned} \quad (14)$$

Here we have used the standard Faddeev-Popov gauge fixing trick, with gauge fixing parameter ξ [28]. Fig. 8 shows the interaction vertices that couple the slow and fast Fourier modes, where the slow modes (to be denoted schematically by $z_{<}$ and $A_{<}$) have momenta in the range $0 < |\vec{k}| < \Lambda/s$ and the fast modes ($z_{>}$ and $A_{>}$) have momenta $\Lambda/s < |\vec{k}| < \Lambda$.

The partition function is separated according to fast and slow modes and the contribution from the fast modes is evaluated perturbatively assuming u , v and e^2 are all of order ϵ .

$$Z = \int \mathcal{D}z_{<}^* \mathcal{D}z_{<} \mathcal{D}A_{<} e^{-S_{<}} \int \mathcal{D}z_{>}^* \mathcal{D}z_{>} \mathcal{D}A_{>} e^{-(V_{<,>} + V_{>,>})} e^{-S_{0,>}}. \quad (15)$$

We have separated out the part of the action which only depends on the slow modes ($S_{<}$), as well as interaction terms in S which mix slow and fast ($V_{<,>}$) and interactions for the fast modes ($V_{>,>}$). Additionally, the part of the action that is quadratic in the fast modes ($S_{0,>}$) is explicitly separated out. The average $\langle e^{-(V_{<,>} + V_{>,>})} \rangle_{0,>}$ can then be computed perturbatively using the cumulant expansion. This leads to a renormalization of the terms in $S_{<}$. To first order in ϵ the renormalized action for the slow modes ($S'_{<}$) looks like

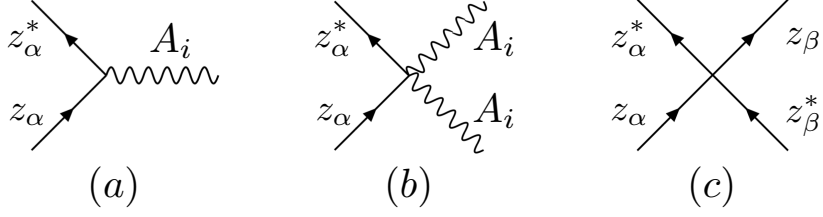


FIG. 8. Interaction vertices that couple fast and slow modes. Perturbative RG is carried out to first order in ϵ by forming all possible one loop diagrams from these vertices.

$$\begin{aligned}
S'_< &= \sum_{\alpha} \int_0^{\Lambda/s} \frac{d\vec{k}}{(2\pi)^d} (\mathcal{Z}_{\eta} \vec{k}^2 + \mathcal{Z}_r r) z_{\alpha}^*(\vec{k}) z_{\alpha}(\vec{k}) \\
&- \mathcal{Z}_{\eta} e \sum_{\alpha} \int_0^{\Lambda/s} \frac{d\vec{k} d\vec{p}}{(2\pi)^{2d}} (2\vec{k} + \vec{p}) \cdot \vec{A}(\vec{p}) z_{\alpha}^*(\vec{p} + \vec{k}) z_{\alpha}(\vec{k}) \\
&+ \mathcal{Z}_{\eta} e^2 \sum_{\alpha} \int_0^{\Lambda/s} \frac{d\vec{k} d\vec{p} d\vec{q}}{(2\pi)^{3d}} \vec{A}(\vec{p}) \cdot \vec{A}(\vec{q}) z_{\alpha}^*(\vec{p} + \vec{q} + \vec{k}) z_{\alpha}(\vec{k}) \\
&+ \frac{1}{2} \sum_{\alpha, \beta} (u' + v' \delta_{\alpha\beta}) \int_0^{\Lambda/s} \frac{d\vec{k}_1 \dots d\vec{k}_4}{(2\pi)^{3d}} \delta^d(\vec{k}_1 - \vec{k}_2 + \vec{k}_3 - \vec{k}_4) z_{\alpha}^*(\vec{k}_1) z_{\alpha}(\vec{k}_2) z_{\beta}^*(\vec{k}_3) z_{\beta}(\vec{k}_4) \\
&+ \frac{1}{2} \sum_{i,j} \int_0^{\Lambda/s} \frac{d\vec{k}}{(2\pi)^d} A_i(\vec{k}) [\mathcal{Z}_A \vec{k}^2 (\delta_{ij} - \hat{k}_i \hat{k}_j) + \frac{k_i k_j}{\xi}] A_j(-\vec{k}),
\end{aligned} \tag{16}$$

where

$$\begin{aligned}
\mathcal{Z}_{\eta} &= 1 - 3\hat{\epsilon}^2 \ln(s) \\
\mathcal{Z}_r &= 1 - [(N+1)\hat{u} + 2\hat{v}] \ln(s) \\
\mathcal{Z}_A &= 1 + \frac{1}{3} N \hat{\epsilon}^2 \ln(s) \\
\hat{u}' &= \hat{u} - [(N+4)\hat{u}^2 + 4\hat{u}\hat{v} + 6\hat{\epsilon}^4] \ln(s) \\
\hat{v}' &= \hat{v} - [5\hat{v}^2 + 6\hat{u}\hat{v}] \ln(s).
\end{aligned} \tag{17}$$

Here we have defined dimensionless couplings $\hat{g} \equiv g\Lambda^{d-4}\mathcal{S}_d/(2\pi)^d$ with \mathcal{S}_d being the surface area of a d -dimensional sphere and $g = e^2, u, v$. We have used Landau gauge $\xi = 0$ (which forces $\vec{\nabla} \cdot \vec{A} = 0$) in order to evaluate loop integrals involving the gauge field propagator. We now rescale the momentum: $\vec{k} \rightarrow \vec{k}/s$ and fields $z_{\alpha}(\vec{k}/s) \rightarrow s^{(d/2+1)} \mathcal{Z}_{\eta}^{-1/2} z_{\alpha}(\vec{k})$, $\vec{A}(\vec{k}/s) \rightarrow s^{(d/2+1)} \mathcal{Z}_A^{-1/2} \vec{A}(\vec{k})$. This defines the renormalized couplings as $r(s) = \mathcal{Z}_r s^2 r / \mathcal{Z}_{\eta}$, $u(s) = u' s^{\epsilon} / \mathcal{Z}_{\eta}^2$, $v(s) = v' s^{\epsilon} / \mathcal{Z}_{\eta}^2$ and $e^2(s) = e^2 s^{\epsilon} / \mathcal{Z}_A$. With the renormalized couplings we can now write the β -functions:

$$\frac{dr}{d\ln s} = r[2 - (N+1)u - 2v + 3e^2] \tag{18a}$$

$$\frac{de^2}{d\ln s} = \epsilon e^2 - \frac{N}{3} e^4 \tag{18b}$$

$$\frac{du}{d\ln s} = \epsilon u - (N+4)u^2 - 4uv - 6e^4 + 6e^2 u \tag{18c}$$

$$\frac{dv}{d\ln s} = \epsilon v - 5v^2 - 6uv + 6e^2 v. \tag{18d}$$

We note that when $N = 1$, these equations have the the same form for v as for u . This is a useful check, as the v term is identical to the u term when $N = 1$. A drawback of the momentum shell approach is that the momentum cutoff breaks gauge invariance, and hence we have discarded terms that would renormalize ξ . The field theoretic RG formulation preserves gauge invariance, and we have checked that our β -functions match using this approach as well.

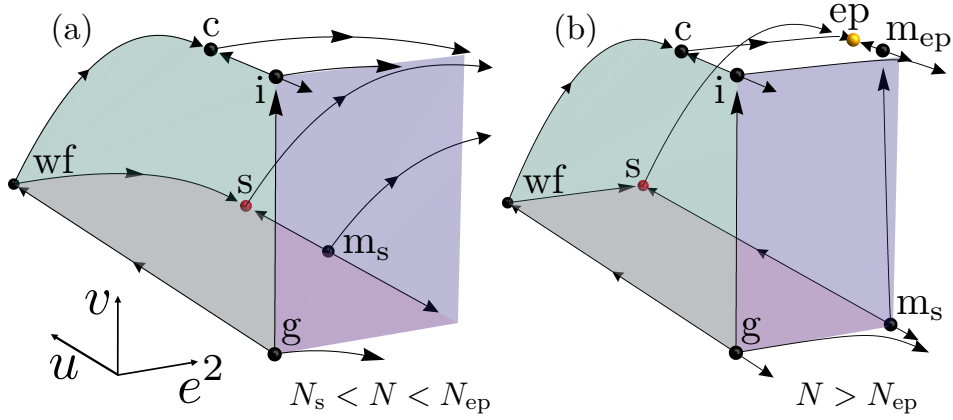


FIG. 9. Here we show our flow diagrams for $N_s < N < N_{ep}$ and $N > N_{ep}$, this time with all of the fixed points marked. The labels correspond to Gaussian (g), Wilson-Fisher (wf), Ising (i), cubic (c), symmetric deconfined (s), symmetric multicritical (m_s), easy-plane deconfined (ep) and easy-plane multicritical (m_{ep}). ep is the only fixed point with all directions irrelevant in the $r = 0$ plane.

RG flow equations

Here we will elaborate on the structure of the RG flow equations that have been presented in the main text. Throughout this discussion, we will take $r = 0$, working in the critical plane. Equation (18b) can be set to zero and solved to find the fixed point values of e^2 . This gives us both charged and uncharged fixed points, $e^2 = 0$ and $e^2 = 3\epsilon/N$. There are always four real fixed points with $e^2 = 0$, which are given by:

$$e^2 = 0 \quad u = 0 \quad v = 0 \quad (19a)$$

$$e^2 = 0 \quad u = \frac{\epsilon}{N+4} \quad v = 0 \quad (19b)$$

$$e^2 = 0 \quad u = 0 \quad v = \frac{\epsilon}{5} \quad (19c)$$

$$e^2 = 0 \quad u = \frac{\epsilon}{5N-4} \quad v = \frac{(N-2)\epsilon}{5N-4}. \quad (19d)$$

These fixed points are identified (see [29]) as Gaussian (19a), Wilson-Fisher or Heisenberg (19b), Ising (19c), and cubic (19d) fixed points. Note that the z fields can be separated into their real and imaginary parts, and when $v = 0$ the same fixed point structure appears as in the $O(2N)$ field theory with quartic interaction $(\sum_{\alpha}^{2N} \phi_{\alpha} \phi_{\alpha})^2$. The addition of v breaks the $O(2N)$ symmetry of the model, since it contains the interaction $\sum_{\alpha}^{2N} \phi_{\alpha}^4$, which is typically referred to as cubic anisotropy. The other fixed point with $v \neq 0$, $u = 0$ is referred to as the Ising fixed point, since it corresponds to $2N$ independent copies of the Ising field theory.

It is well known that in the $O(n)$ model (to first order in ϵ) the Wilson-Fisher fixed point is stable for $n < 4$, and for $n > 4$ the cubic fixed point becomes the only stable one. In our case $2N = n$, and we indeed observe exactly this behavior in our flow equations below and above $N = 2$.

We now go on to discuss the fixed points when $e^2 = 3\epsilon/N$. The two fixed points with $v = 0$ are given by:

$$\begin{aligned} e^2 &= 3\epsilon/N \\ u_{\pm} &= \frac{\epsilon}{2N(N+4)} \left(N + 18 \pm \sqrt{(N+18)^2 - 216(N+4)} \right) \\ v &= 0. \end{aligned} \quad (20)$$

These two fixed points become real when $N > 182.9516 = N_s$. Of these, the fixed point at u_+ is the symmetric deconfined fixed point, which is stable in the $r = 0, v = 0$ plane. The multicritical point at u_- has one relevant direction in the $r = 0, v = 0$ plane. We note that when $v \neq 0$, this causes a runaway flow from the deconfined fixed point, which shows up as a first order transition in our lattice simulations. For this value of N (corresponding to panel (a) of Fig. 9) there are no stable fixed points in the $r = 0$ plane.

We now move to the final fixed points that appear as N is increased even further, which is the main result of this paper. This corresponds to the finite solution for v in Eqn (18d)

$$\begin{aligned}
 e^2 &= 3\epsilon/N \\
 u_{\pm} &= \frac{\epsilon}{2N(5N-4)} \left(N + 18 \pm \sqrt{(N+18)^2 - 1080(5N-4)} \right) \\
 v_{\pm} &= \frac{1}{5} [\epsilon(1 + 18/N) - 6u_{\pm}]
 \end{aligned} \tag{21}$$

Here the solutions for u (and hence the solutions for v) become real when $N > 5363.1341 = N_{\text{ep}}$. The solution at u_+ is the easy-plane deconfined fixed point, which has all directions irrelevant in the $r = 0$ plane and is hence stable. The other solution at u_- is a multicritical point denoted by m_{ep} in Fig. 9. The easy-plane deconfined fixed point describes the criticality observed in our lattice model at large N .

We note at this point that the values of N_s and N_{ep} obtained from the ϵ expansion at first order are notoriously unreliable. The value of N_s is believed to extend all the way down to $N = 2$ based on the observed deconfined criticality in spin-1/2 systems [1]. Likewise we observe $N_{\text{ep}} \approx 20$ from our lattice simulations. It is interesting to note that the ϵ expansion gives N_{ep} that is an order of magnitude larger than N_s , which is observed in numerical simulations.